

Dynamical evolution of fermion-boson stars

Susana Valdez-Alvarado¹, Carlos Palenzuela², Daniela Alic³, L. Arturo Ureña-López¹

¹*Departamento de Física, DCI, Campus León, CP 37150,
Universidad de Guanajuato, León, Guanajuato, México,*

²*Canadian Institute for Theoretical Astrophysics, Toronto, Ontario M5S 3H8, Canada,*

³*Max-Planck-Institut für Gravitationsphysik, Albert-Einstein-Institut, Potsdam-Golm, Germany*

Compact objects, like neutron stars and white dwarfs, may accrete dark matter, and then be sensitive probes of its presence. These compact stars with a dark matter component can be modeled by a perfect fluid minimally coupled to a complex scalar field (representing a bosonic dark matter component), resulting in objects known as fermion-boson stars. We have performed the dynamical evolution of these stars in order to analyze their stability, and to study their spectrum of normal modes, which may reveal the amount of dark matter in the system. Their stability analysis shows a structure similar to that of an isolated (fermion or boson) star, with equilibrium configurations either laying on the stable or on the unstable branch. The analysis of the spectrum of normal modes indicates the presence of new oscillation modes in the fermionic part of the star, which result from the coupling to the bosonic component through the gravity.

I. INTRODUCTION

Scalar fields are of great interest in several fields of physics. In high energy physics they arise naturally in several unification theories, such as scalar-tensor theories of gravitation from string theory. In cosmology, they have been considered to provide inflationary solutions in the early universe and an alternative explanation for dark energy. In addition, they have also been proposed as strong candidates of dark matter, the matter that is responsible for the formation and evolution of structures in the Universe. For the latter type of models, one of the possibilities assumes that dark matter is composed by bosonic particles which may condensate into macroscopic self-gravitating objects (i.e., self-gravitating Bose-Einstein condensates) commonly known as *boson stars*. Since the seminal paper in the late sixties by Ruffini and Bonazzola [1], boson stars in General Relativity have been extensively studied in many different contexts (for a recent review see [2]).

On the other hand, the formation of either a boson or a fermion star would be susceptible to subsequent mixture by fermions/bosons, and this fact opens a whole new possibility for the formation of objects made of both fermionic and bosonic particles. Even if one of these objects is formed in a medium absent of either bosonic or fermionic particles, the latter may be accreted in later stages. In particular, bosonic dark matter particles may accrete on compact stars, and depending on the model considered, their effects on the star will be different and possibly observable.

In the context of WIMPs, if the dark matter is self-annihilating, the released energy due to the WIMP annihilation inside the neutron star can increase the temperature and be observable in old stars [3]. If it does not self-annihilate, the dark matter will cluster in a small region at the center of the neutron star, increasing their compactness and ultimately leading to a gravitational collapse [4]. Neutron stars may be therefore sensitive indirect probes of the presence of dark matter, and can

be used to set constraints both on the density and on the physical properties of dark matter.

Recent studies investigate possible changes in the structure of the star in the presence of dark matter, by using a two-fluid model [5]. In this paper, we perform a similar analysis by modeling systems which contain a fermionic compact star (we consider it to be a neutron star) and a bosonic dark matter component represented by a boson star. The resulting objects are known as fermion-boson stars. These mixed stars were first introduced by Henriques et. al. [6] (and further studied in [7, 8]), where the fermionic matter was described by a perfect fluid with the Chandrasekhar equation of state, while the bosonic component is modeled by using a real quantized scalar field as in [9]. The bosons and the fermion particles are coupled only through gravity (notice however that non-minimal couplings with the scalar field can arise in other scenarios, such as in neutron stars with hidden extra dimensions [10] or in tensor-scalar theories of gravitation [11]). We will perform a dynamical analysis of these mixed stars by using a simple polytropic equation of state, as it is standard for cold neutron stars, and a complex scalar field to describe the bosonic component.

The equilibrium configurations for either an isolated boson or fermion stars are described, respectively, by the central value of the scalar field ϕ_c , and the central value of the fluid density ρ_c [1, 12]. These configurations are therefore characterized by a single parameter σ_c , so in this case there are stability theorems [13, 14] which indicate that the critical mass (separating the unstable from the stable branch) is located at the extrema $\partial M/\partial \sigma_c = 0$. However, the mixed fermion-boson stars are parameterized not by one, but by two quantities (ϕ_c, ρ_c) . This implies that the analysis of stability is more complicated than in the isolated star case, since the previous stability theorems can not be directly applied. One can still analyze their stability, among other alternatives, by studying the radial perturbations of these equilibrium configurations and then analyzing the eigenvalues of these modes

in the linearized equations as in [15–19], or by evolving dynamically these perturbations by solving the full non-linear equation of motion [20–23]. In [24, 25] Henriques et al. described a method to perform the analysis of stability of the boson-fermion stars by using the binding energy and the number of bosonic and fermionic particles as a function of the two free parameters. In this paper, we propose a similar criterion, and our results are compared with the full numerical solution of the equations of motion. In addition to the stability analysis, we follow the migration of a star from an unstable to the stable branch, a process observed already in isolated boson and fermion stars. Finally, we study the dependence of the quasi-normal modes of the mixed star with respect to their fraction of bosonic matter.

The paper is organized as follows. In Sec. II we introduce the formalism used to obtain the set of evolution equations that describes the spacetime geometry and the boson-fermion matter contents. In Sec. III we describe how to construct the initial data for the boson-fermion stars, and propose a method to find the stability of these objects. The results of the dynamical evolution for equilibrium configurations (i.e., both stable and unstable) are presented in Sec. IV, together with the spectrum of the quasi-normal modes of the stable stars. Finally, conclusions and final remarks are presented in Sec. V. Throughout this paper we use that the indices are a, b, \dots taken to run from 0 to 3, while indices i, j, \dots run from 1 to 3. We also adopt the standard convention for the summation over repeated indices.

II. FORMALISM

Fermions minimally coupled to bosons can be modeled by considering a stress-energy tensor with contributions from a perfect fluid and a complex scalar field, in the form

$$T_{ab} = T_{ab}^{(\text{fluid})} + T_{ab}^{(\phi)}, \quad (1)$$

$$T_{ab}^{(\text{fluid})} = [\rho_o (1 + \epsilon) + P] u_a u_b + P g_{ab}, \quad (2)$$

$$T_{ab}^{(\phi)} = \frac{1}{2} [\partial_a \phi^* \partial_b \phi + \partial_a \phi \partial_b \phi^*] - \frac{1}{2} g_{ab} [\partial^\alpha \phi^* \partial_\alpha \phi + m^2 |\phi|^2]. \quad (3)$$

The perfect fluid is represented by the fermionic physical (primitive) variables, namely the pressure P , rest-mass density ρ_o , internal energy ϵ , and four-velocity u^a , whereas the complex scalar field ϕ describes a Bose-Einstein condensate of bosonic particles of mass m . The fluid and the scalar field do not interact directly, and are only coupled through gravity, as it is expected for WIMPS. The equations of motion for the fluid and the scalar field are obtained from *the conservation laws* of the stress-energy tensor and the baryonic number

$$\nabla_a T_{(\text{fluid})}^{ab} = 0, \quad \nabla_a (\rho_o u^a) = 0, \quad (4)$$

and the Klein-Gordon equation

$$\nabla_a \nabla^a \phi = m^2 \phi, \quad (5)$$

which together with the Einstein equations $G_{ab} = 8\pi T_{ab}$ constitute the system of equations governing the dynamics.

We restrict our study to spherically symmetric stars, and then consider the time-dependent metric

$$ds^2 = -\alpha^2(t, r) dt^2 + g_{rr}(t, r) dr^2 + r^2 g_{\theta\theta}(t, r) d\Omega^2. \quad (6)$$

The evolution equations for the spacetime are obtained by considering the $Z3$ formulation of the Einstein equations [26], which introduces the following independent quantities to form a first order system of equations,

$$\begin{aligned} A_r &= \frac{\partial_r \alpha}{\alpha}, \quad D_{rr}{}^r = \frac{g^{rr}}{2} \partial_r g_{rr}, \quad D_{r\theta}{}^\theta = \frac{g^{\theta\theta}}{2} \partial_r g_{\theta\theta}, \\ K_r{}^r &= -\frac{1}{2\alpha} \frac{\partial_t g_{rr}}{g_{rr}}, \quad K_\theta{}^\theta = -\frac{1}{2\alpha} \frac{\partial_t g_{\theta\theta}}{g_{\theta\theta}}. \end{aligned} \quad (7)$$

The full system of equations for this formulation is included in appendix A. The remaining freedom in the choice of coordinates of the line element (6) is related to the prescription for the lapse function, and a common option is the harmonic slicing condition

$$\partial_t \alpha = -\alpha^2 \text{tr} K, \quad (8)$$

where $\text{tr} K = K_r{}^r + 2K_\theta{}^\theta$. By using the metric (6), the equations of motion for the perfect fluid (4) and the scalar field (5) can be written explicitly as:

$$\partial_t(\sqrt{\gamma} D) = -\partial_r(\sqrt{\gamma} \alpha v^r D) - \frac{2}{r} \sqrt{\gamma} \alpha v^r D, \quad (9a)$$

$$\partial_t(\sqrt{\gamma} U) = -\partial_r(\sqrt{\gamma} \alpha \tilde{S}^r) + \sqrt{\gamma} \alpha \left[\tilde{S}_r{}^r K_r{}^r + 2\tilde{S}_\theta{}^\theta K_\theta{}^\theta - \tilde{S}^r \left(\frac{2}{r} + A_r \right) \right], \quad (9b)$$

$$\partial_t(\sqrt{\gamma} \tilde{S}_r) = -\partial_r(\sqrt{\gamma} \alpha \tilde{S}_r{}^r) + \sqrt{\gamma} \alpha \left[\tilde{S}_r{}^r \left(D_{rr}{}^r - \frac{2}{r} \right) + 2\tilde{S}_\theta{}^\theta \left(\frac{1}{r} + D_{r\theta}{}^\theta \right) - U A_r \right], \quad (9c)$$

$$\partial_t \phi_t = \partial_r(\alpha \sqrt{g^{rr}} \phi_r) + \alpha \sqrt{g^{rr}} \left[2 \left(D_{r\theta}{}^\theta + \frac{1}{r} \right) \phi_r + 2\sqrt{g_{rr}} K_\theta{}^\theta \phi_t - m^2 g_{rr} \phi \right], \quad (9d)$$

where $\sqrt{\gamma} = \sqrt{g_{rr}g_{\theta\theta}}$ and we have introduced the auxiliary fields

$$\phi_r = \partial_r \phi, \quad \phi_t = \frac{\sqrt{g_{rr}}}{\alpha} \partial_t \phi, \quad (10)$$

to reduce the Klein-Gordon equation to first order in space and time.

The evolution of the fluid is described in terms of the *conserved* variables, namely the mass density D , the momentum density \tilde{S}_r and the energy density U . They are related to the primitive variables (i.e., the rest-mass density ρ_o , the pressure P and the velocity v_r) by the following relations

$$D = \rho_o W, \quad U = hW^2 - P, \quad \tilde{S}_r = hW^2 v_r, \quad (11)$$

where $h = \rho_o(1 + \epsilon) + P$ is the enthalpy and $W = 1/\sqrt{1 - v^r v_r}$ the Lorentz factor. In the right-hand-side of their evolution equations, the spatial projections of the stress-energy tensor take the form,

$$\tilde{S}_r{}^r = hW^2 v_r v^r + P, \quad \tilde{S}_\theta{}^\theta = P.$$

During the evolution, the relations (11) must be inverted in order to obtain the primitive physical quantities

(which are necessary for computing the rhs) from the conserved evolved fields. In general, this conversion can not be performed analytically, so appendix B explains in detail our numerical algorithm for obtaining the primitive fields.

III. INITIAL DATA

Initial data for the fermion-boson stars involves the intrinsic metric g_{ij} and extrinsic curvature K_{ij} on a given hyper-surface, as well as the fermionic fluid configuration in terms of its primitive variables (ρ, ϵ, v^i) and the bosonic scalar field ϕ . Assuming a static spherically symmetric metric in Schwarzschild coordinates

$$ds^2 = -\alpha^2(r) dt^2 + a^2(r) dr^2 + r^2 d\Omega^2, \quad (12)$$

a harmonic form of the scalar field $\phi(t, r) = \phi(r)e^{-i\omega t}$ [44], and a star in hydrostatic equilibrium with $v_r = 0$, the following system of ODEs is obtained:

$$\frac{da}{dr} = \frac{a}{2} \left\{ \frac{1}{r}(1 - a^2) + 4\pi G r \left[\left(\frac{\omega^2}{\alpha^2} + m^2 \right) a^2 \phi^2(r) + \Phi^2(r) + 2a^2 \rho(1 + \epsilon) \right] \right\}, \quad (13a)$$

$$\frac{d\alpha}{dr} = \frac{\alpha}{2} \left\{ \frac{1}{r}(a^2 - 1) + 4\pi G r \left[\left(\frac{\omega^2}{\alpha^2} - m^2 \right) a^2 \phi^2(r) + \Phi^2(r) + 2a^2 P \right] \right\}, \quad (13b)$$

$$\frac{d\phi}{dr} = \Phi(r), \quad (13c)$$

$$\frac{d\Phi}{dr} = \left(m^2 - \frac{\omega^2}{\alpha^2} \right) a^2 \phi - [1 + a^2 - 4\pi G a^2 r^2 (m^2 \phi^2 + \rho(1 + \epsilon) - P)] \frac{\Phi}{r}, \quad (13d)$$

$$\frac{dP}{dr} = -[\rho(1 + \epsilon) + P] \frac{\alpha'}{\alpha}. \quad (13e)$$

The system is completed by choosing the equation of state (EoS) that relates the pressure with the other fluid quantities. As it is standard in simple models of cold stars, we will adopt here a polytropic equation of state $P = K\rho^\Gamma$, with the particular choice of $\Gamma = 2$ and $K = 100$, which corresponds to masses and compactness in the range of neutron stars [12].

We will use units such that $c = 1$, and the variables can be renormalized to absorb the factors G and m , so that the basic scale of the stars will be given by $\{K, \Gamma\}$. The final system is an eigenvalue problem for the frequency of the boson star ω as a function of two parameters; the central value of the scalar field ϕ_c and the density of the fluid ρ_c . This system can be solved by using the Shooting Method [27].

The appropriate boundary conditions for the scalar field and metric functions are obtained by imposing the conditions of regularity at the origin and asymptotic flatness at infinity. The condition at $r = 0$ for the fluid pressure is obtained from the polytropic EoS as a function of ρ_c . Thus, the full boundary conditions are

$$a(0) = 1, \quad \alpha(0) = 1, \quad \phi(0) = \phi_c, \quad (14a)$$

$$\Phi(0) = 0, \quad P(0) = K\rho_c^\Gamma, \quad (14b)$$

$$\lim_{r \rightarrow \infty} \alpha(r) = \lim_{r \rightarrow \infty} \frac{1}{a(r)}, \quad (14c)$$

$$\lim_{r \rightarrow \infty} \phi(r) \approx 0, \quad \lim_{r \rightarrow \infty} P(r) = 0. \quad (14d)$$

After the solution is found, a change of coordinates from Schwarzschild to maximal isotropic ones is per-

formed

$$ds^2 = -\alpha^2(\tilde{r})d\tilde{t}^2 + \psi^4(\tilde{r}) (d\tilde{r}^2 + \tilde{r}^2 d\Omega^2), \quad (15)$$

which are more convenient for our numerical evolution and for future comparisons in three dimensions. All of our simulations will be shown in these coordinates, and for simplicity we will substitute $\tilde{r} \rightarrow r$ hereafter.

The total gravitational mass is computed by the asymptotic value of the metric coefficients

$$M_T = \lim_{r \rightarrow \infty} \frac{r}{2} \left(1 - \frac{1}{\alpha^2} \right). \quad (16)$$

The $U(1)$ symmetry in the Lagrangian of the scalar field ensures the conservation of a Noether charge which can be associated with the number of bosons N_B [23, 24]. Correspondingly, the conservation of baryonic number allows to define a number of fermions N_F . These quantities can be computed by integrating their densities,

$$\frac{\partial N_B}{\partial r} = \frac{4\pi a \omega \phi^2 r^2}{\alpha}, \quad \frac{\partial N_F}{\partial r} = 4\pi a \rho r^2. \quad (17)$$

Therefore, the radius of the fermionic/bosonic parts of the star can be defined as the surface containing 99% of the corresponding particles.

A. Boson and fermion stars

As a basic test of our initial data implementation we compare our equilibrium configurations with previously published results for isolated boson stars and fermion stars, which are the limits of our system of equations when $\rho_c \rightarrow 0$ and $\phi_c \rightarrow 0$ respectively.

Fig. (1) shows the total mass M_T of boson stars and fermion stars as a function of the corresponding radius R_{99} . In agreement with the results of previous works, we have found that the maximum mass M_{max} (i.e., the value of the mass that separates the stable $M_T < M_{max}$ from the unstable $M_T > M_{max}$ configurations) in the case of boson stars is $M_{max} = 0.633$, whereas for fermionic stars is $M_{max} = 1.637$ with $\Gamma = 2$ and $K = 100$.

B. Mixed boson-fermion stars

As we mentioned before, the equilibrium configurations of mixed boson-fermion stars are more involved and depend on the two parameters ϕ_c and ρ_c . The total mass of the stars as a function of these parameters is plotted in Fig. 2, showing that the maximum mass is obtained for the isolated neutron star case (i.e., when $\phi_c = 0$). This is a direct consequence of our choice of the parameters $\{K, \Gamma\}$ in the equation of state, that sets the scale and the compactness of the mixed stars. With the current choice, the stars will be composed predominantly by fermions, which can produce stars with much higher compactness than boson stars.

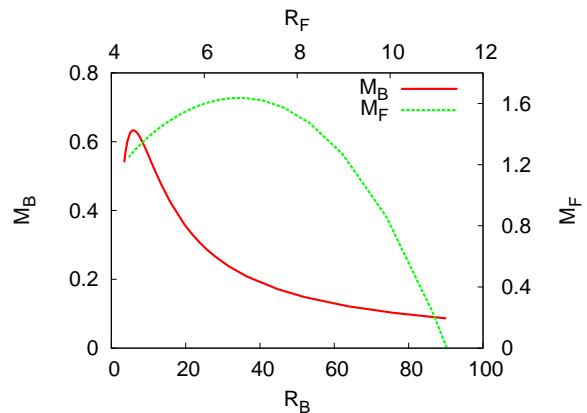


FIG. 1: *Initial data of isolated stars.* The total masses of the boson M_B and fermion M_F stars, as functions of their corresponding radius R_{99} . The maximum mass agrees in each case with previous results found in the literature, namely $M_{max} = 0.633$ for boson stars, and $M_{max} = 1.637$ for fermion stars.

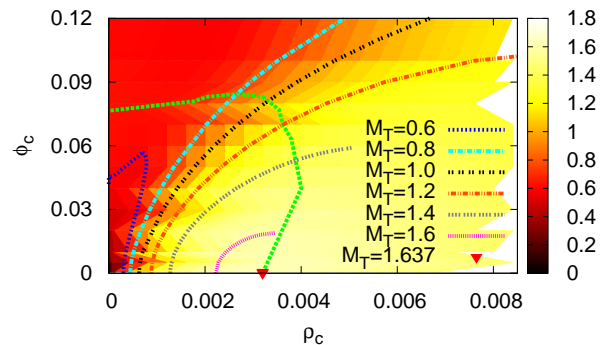


FIG. 2: *Initial data of mixed fermion-boson stars.* The total mass of the equilibrium configurations of the mixed stars, M_T , as a function of ϕ_c and ρ_c . The maximum mass, for a given value of ρ_c , is always found when $\phi_c = 0$, implying that $M_{max} = 1.637$ is the maximum mass value for any boson-fermion star in this study. The (green) solid line that intersects the axes is the stability boundary discussed in the text, see also Fig. 5.

The profiles of the different non-trivial fields for a representative case are plotted in Fig. 3, which clearly satisfy the regularity conditions at the origin and asymptotic flatness. The presence of the fermionic fluid produces a deeper gravitational potential than the one produced solely by the boson star, therefore contracting the bosonic component to a smaller radius, comparable to the one of the fermionic matter.

For a fixed value of the total mass M_T , we find that the number of bosons N_B increases for $\phi_c \geq 0$, reaches a maximum, and then decreases. Notice that since the total mass is kept fixed, the central density ρ_c must change

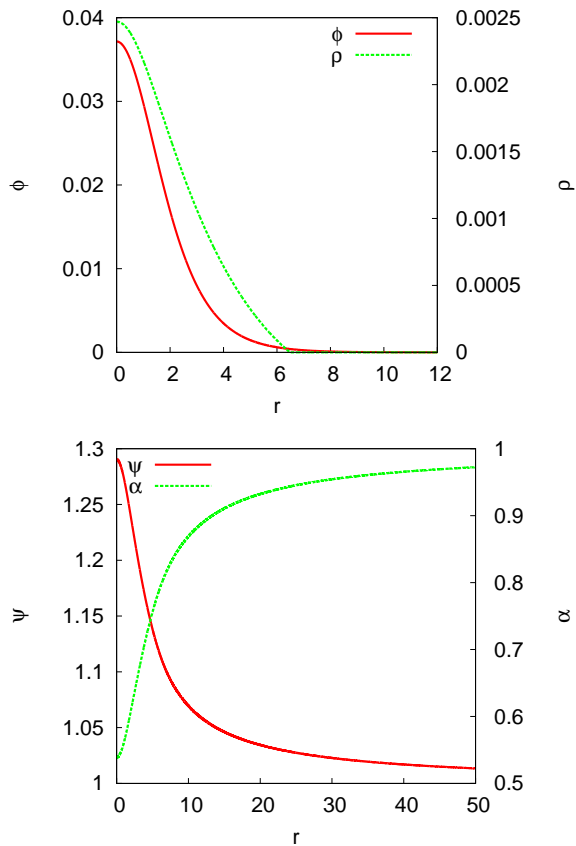


FIG. 3: *Initial data of mixed fermion-boson stars.* The profiles of the scalar field $\phi(r)$, the fermionic density $\rho(r)$, and the conformal factor $\psi(r)$ for one typical configuration corresponding to $N_B/N_F = 0.1$ and $M_T = 1.4$.

as we vary ϕ_c . The number of fermions N_F has consequently the complementary behavior to that of N_B : it decreases until reaching a minimum and then increases. The same profiles are observed in these quantities when they are represented as a function of ρ_c instead of ϕ_c . This behavior is illustrated in Fig. 4, where the number of particles is plotted as a function of ϕ_c and ρ_c for the configurations with mass $M_T = 1.4$.

Following usual nomenclature, we call 'critical point' an equilibrium fermion-boson solution – described by $\{M, N_F, N_B\}$ – which separates the stable from the unstable configurations. This transition is signaled by the passing through zero of the lowest eigenvalue in the (radial) perturbations of the fermion-boson star.

The stability analysis for the boson-fermion stars, which can be performed for instance by solving the perturbed equations of motion, is much more complicated than for isolated boson or fermion stars (see for instance [7, 8, 24, 25]). The main reason, as it was mentioned before, is that these mixed configurations have two free parameters (i.e., the central values of the scalar field ϕ_c and the density of the perfect fluid ρ_c) instead of just one, so that the stability theorems for a single parameter

solutions can not be directly applied.

Instead of performing again this stability analysis, we propose a different way to find critical configurations. Our criterion is based on the studies made in [24], in which the authors realized that in a critical point (i.e., where the eigenvalue of the perturbation vanishes) there must be a direction \mathbf{n} such that the directional derivatives of $\{M, N_F, N_B\}$ vanish

$$\left. \frac{dM}{d\mathbf{n}} \right|_b = \left. \frac{dN_B}{d\mathbf{n}} \right|_b = \left. \frac{dN_F}{d\mathbf{n}} \right|_b = 0, \quad (18)$$

where the subscript b means the value of the quantities at the critical point. The direction \mathbf{n} at the stability boundary is tangential to the level curves of constant M , N_B , and N_F ; formally speaking, the direction \mathbf{n} is orthogonal to the gradient of the functions at the boundary, $\mathbf{n} \perp \nabla(M_T, N_B, N_F)|_b$. Therefore, the stability boundary can be found by drawing contours onto the plane (ϕ_c, ρ_c) for fixed values of the particle numbers, and looking for the points where these curves meet and are tangential one to each other; this was method used in [24].

In addition, we have noticed –as also did the authors in [24]– that the curves of constant mass M_T osculates the curves of constant particle numbers, so that the stability boundary can be found by surveying the behavior of N_B and N_F while keeping fixed the value of M_T . More precisely, a level curve of constant total mass, $M_T(\rho_c, \phi_c) = M_0$, implicitly defines the trajectory $\phi_c = \phi_c(\rho_c, M_0)$, and then the derivatives of the particle numbers along this given trajectory are

$$\frac{dN_B}{d\rho_c} = [\nabla N_B \cdot \mathbf{s}](\rho_c), \quad \frac{dN_F}{d\rho_c} = [\nabla N_F \cdot \mathbf{s}](\rho_c),$$

where $\mathbf{s}(\rho_c) = (1, d\phi_c/d\rho_c)$ is the velocity vector of the level curve $\phi_c = \phi_c(\rho_c, M_0)$ at any given point. As we approach the boundary line $\mathbf{s} \rightarrow \mathbf{n}$, the derivatives in Eqs. (19) must vanish at the critical point as stated by Eqs. (18). Consequently, the equilibrium critical configurations manifest themselves at the extreme values of the number of particles when surveyed along a level curve of constant total mass.

For the particular case $M_T = 1.4$ displayed in Fig. 4, the critical configuration is obtained when $N_B = 0.163$ and $N_F = 1.37$. We can see that the critical point also corresponds to a maximum of the boson-fermion ratio N_B/N_F , whose critical value for $M_T = 1.4$ is $N_B/N_F = 12\%$. We applied this recipe for values in the range $0.633 \leq M_T \leq 1.637$, where the limiting values are established by the critical boson and fermion cases, respectively, and the solution space of stable/unstable configurations using this criterion is shown in Fig. 5. As noted before in [24], stable configurations lie inside this boundary line, where the known stable cases of boson and fermion stars are found.

Notice that the procedure described above is quite general, and we could have used the level curves of any of the functions involved. For instance, if we would have taken

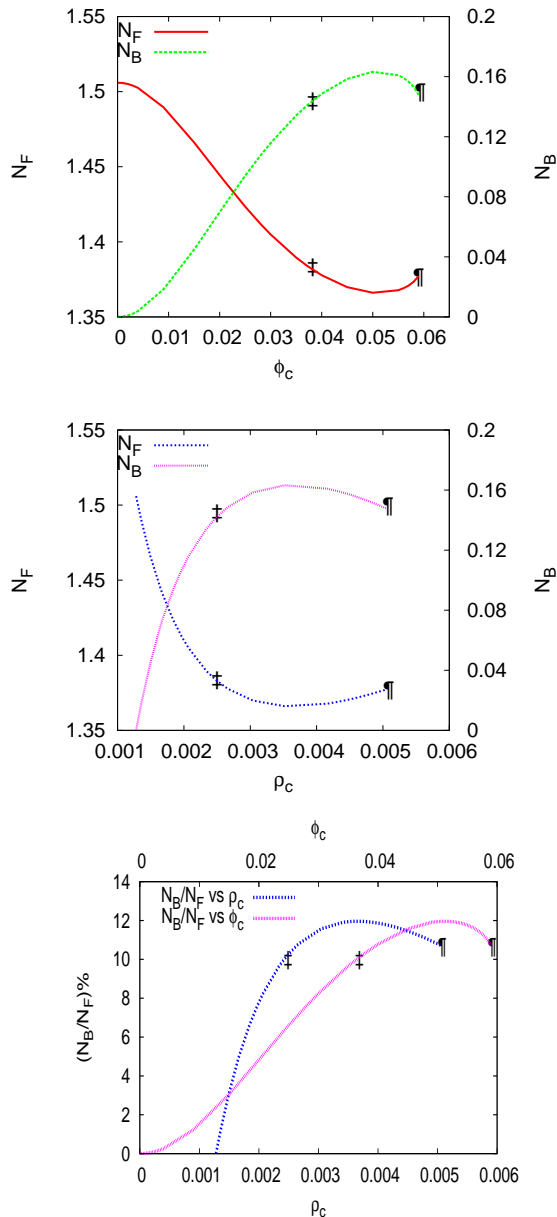


FIG. 4: *Initial data of mixed fermion-boson stars.* The number of fermions N_F and bosons N_B for the equilibrium configurations as a function of ϕ_c (top panel) and ρ_c (middle panel) corresponding to the fixed total mass $M_T = 1.4$. The position of the maximum/minimum corresponds to the critical point which separates the stable and the unstable solutions. The two configurations considered in the next section are marked, one on each side of the maximum/minimum, corresponding to $N_B = 10\%N_F$ (\dagger) and $N_B = 10.7\%N_F$ (\ddagger). (Bottom panel) The boson-to-fermion ratio, N_B/N_F for $M_T = 1.4$; the critical configuration corresponds to the maximum value $N_B/N_F = 12\%$.

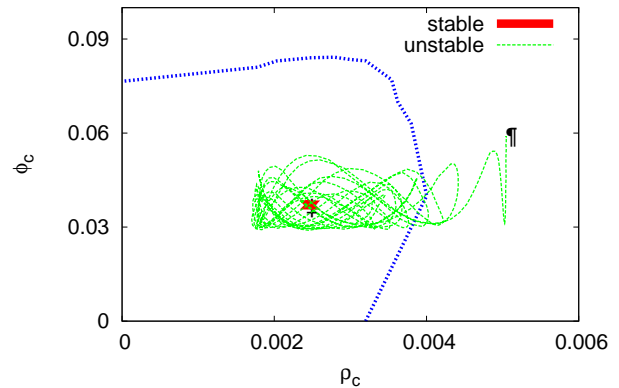


FIG. 5: *Initial data of mixed fermion-boson stars.* Regions of stability/instability for the equilibrium configurations of the mixed boson-fermion stars, according to the criterion of maximum/minimum of the number of bosons/fermions for a fixed M_T , see also Fig. 4 and the text for more details. Notice that the values at the axes coincide with the fermion and boson expected critical values, which are $\rho_c = 3.2 \times 10^{-3}$, and $\phi_c = 7.65 \times 10^{-2}$, respectively. We mark the two configurations corresponding to $N_B = 10\%N_F$ (\dagger) and $N_B = 10.7\%N_F$ (\ddagger), whose stability is studied numerically in Figs. 6 and 8, respectively. The first one is stable and remains in the same state (point), whereas the second is unstable and migrates towards the stable region.

the level curve for $N_B(\rho_c, \phi_c) = N_0$, we could have surveyed M_T, N_F and found that the critical configuration corresponds to their extreme values. Moreover, either ρ_c or ϕ_c could have been used as the independent variable, as it is shown in Fig. 4.

Summarizing, our criterion is based on the analytical work in [24], but takes advantage of the fact that critical configurations appear as critical points of the particle numbers when the total mass is held fixed. The configurations with the number of bosons (fermions) on the left of the maximum (minimum) are stable configurations, while configurations that are on the right of the maximum (minimum) are unstable. These results are validated through numerical simulations presented in the next section, where we describe the evolution of the two equilibrium configurations marked with symbols in Fig. 4, one with $N_B = 10\%N_F$, which is on the left of the critical ratio, and another with $N_B = 10.7\%N_F$, which is on the right of the critical ratio. Our simulations show that the first configuration is stable (i.e., small perturbations are bounded, and the system remains in the same state throughout the entire evolution), whereas the second one is unstable and the system changes to a different configuration.

This behavior is also shown in Fig. 5 where we can see that the stable configuration stays in the stable region, while the unstable configuration leaves the unstable region and migrates towards the stable one. This suggests that the maximum/minimum values of the afore-

mentioned curves may mark the existence of a critical configuration for a given fixed mass.

IV. NUMERICAL SIMULATIONS

In this section we analyze the dynamics of mixed stars, and address different issues like the stability of these systems or their spectrum of normal modes. In order to determine the properties of the mixed star equilibrium configurations described in the previous section, we performed long-term numerical evolutions of the discretized Einstein-Klein-Gordon-Hydrodynamic system (9).

We write the system in flux conservative form

$$\partial_t \mathbf{U} + \partial_k F^k(\mathbf{U}) = S(\mathbf{U}), \quad (19)$$

so that we can apply numerical algorithms based on Finite Volume methods. The spatial discretization of the geometry and the boson fields is performed using a third order accurate Finite Volume method [26], which can be viewed as a fourth order finite difference scheme plus third order adaptive dissipation. The dissipation coefficient is given by the maximum propagation speed in each grid point. For the fluid matter fields, we use a High Resolution Shock Capturing method with Monotonic-Centered limiter. The time evolution is performed through the method of lines using a third order accurate Strong Stability Preserving Runge-Kutta integration scheme [28], with a Courant factor of $\Delta t/\Delta r = 0.25$ so that the Courant-Friedrichs-Lewy (CFL) condition dictated by the principal part of the equations is satisfied. Most of the simulations presented in this work have been done with a spatial resolution of $\Delta r = 0.01$, in a domain with outer boundary situated at $r = 600$. We use maximally dissipative boundary conditions for the spacetime variables and the boson fields, and outflow boundaries for the fluid matter fields.

A. Stable boson-fermion stars

The dynamical evolution of the mixed equilibrium solution corresponding to $N_B = 10\%N_F$ and total mass $M_T = 1.4$, is shown in Fig. 4. Since it is located on the left of the critical values, we expect this configuration to be stable.

The evolution displays a combination of the behaviors that are typical for isolated boson and fermion stars. The scalar field oscillates with its characteristic eigenfrequency, while the fluid density oscillates slightly around its initial state due to the perturbation introduced by the numerical truncation errors. The values of the peaks of the oscillatory scalar field ϕ_0^{max} and the fluid density ρ_0 at the center of the star are plotted as a function of time in the top panel of Fig. 6, while the total mass M_T and the number of particles N_B , N_F are displayed in the bottom panel.

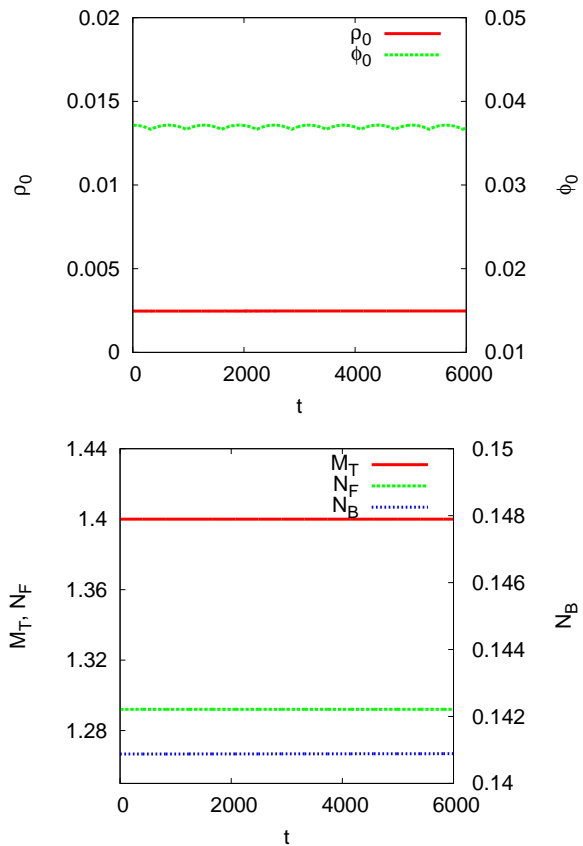


FIG. 6: *Evolution of stable fermion-boson stars* The central values of the density and the (peaks of the oscillatory) scalar field (top), and the mass and the number of bosonic and fermionic particle (bottom). All the quantities remain very close to their initial values, suggesting that the star is stable against perturbations.

These quantities remain very close to their initial value for many dynamical times (except for a tiny drift due to numerical dissipation), indicating that the configuration is indeed stable. In order to assess the robustness and accuracy of our numerical implementation, we have evolved this configuration with three different spatial resolutions $\Delta r = (0.02, 0.01, 0.005)$, in a domain of $r = 600$, for $t \approx 2000$, finding that the numerical solution converges at second order. The energy constraint (A1) is small during the evolution and converges to zero, as it is shown in Fig. 7.

B. Unstable boson-fermion stars

The numerical evolution of the equilibrium configuration with $N_B = 10.7\%N_F$ and $M_T = 1.4$ presents a more dynamical behavior. This configuration lies on the right of the critical values of the number of particles N_F and N_B in Fig. 4, indicating that it is unstable under perturbations.

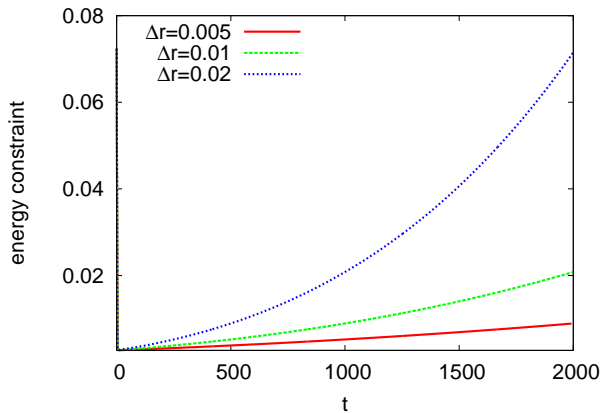


FIG. 7: The energy constraint (A1) for three different resolutions $\Delta r = 0.005$ (red), $\Delta r = 0.01$ (green), and $\Delta r = 0.02$ (blue), showing second order convergence.

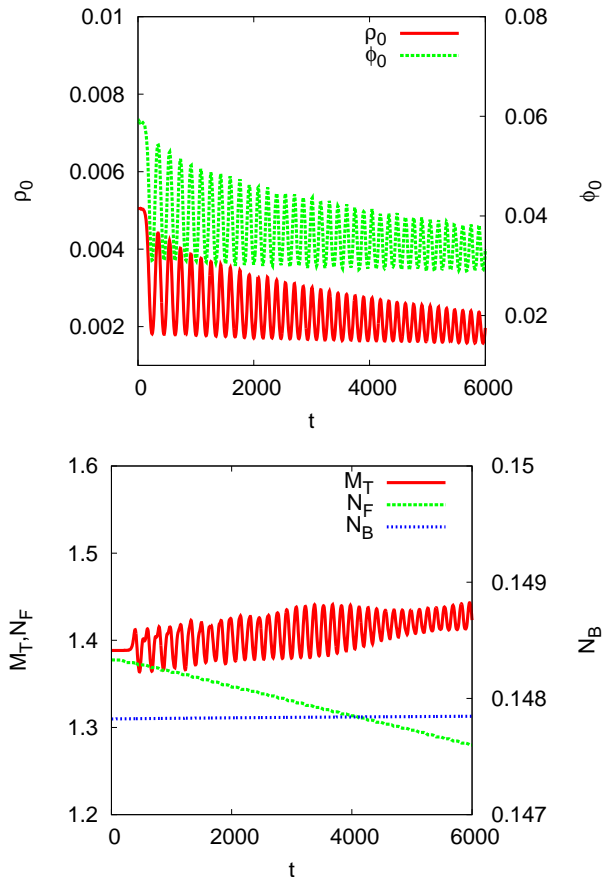


FIG. 8: *Evolution of unstable fermion-boson stars* Same as fig. 6 for a star on the right of the critical curve. The central values of the density and (the peaks of) the scalar field depart quickly from their initial values, indicating that the star is unstable. The evolution becomes non-linear and describes the migration of the star from the unstable to the stable branch.

The initial stage of the evolution is similar to the pre-

vious case of a stable star, with the scalar field oscillating mainly with its eigenfrequency, and the neutron star oscillating due to the perturbation introduced by the inherent numerical truncation errors. However, these oscillations grow rapidly in amplitude, driving the dynamics to a non-linear regime; the star is eventually migrating from the unstable to the stable branch. The central values ρ_0 and the maximum ϕ_0^{max} , the total mass M_T , and the number of particles N_B and N_F , are plotted in Fig. 8. The central values show large variations which are damped slowly, and finally will settle down onto a new stable configuration with practically the same number of bosonic and fermionic particles.

Notice however that the large oscillations in the central density induces significant variations with the same frequency in the radius of the star. The interaction of the expanding and contracting star's surface with the atmosphere (i.e., the low density fluid populating the star's exterior) produces an artificial small loss of the baryonic mass during the migration that can be observed in Fig. 8.

C. Quasi-Normal Modes of the stable stars

As it has already been mentioned, the fermion-boson star will oscillate around its stable configuration due to the perturbations introduced by the numerical truncation errors, in a similar way as an isolated fermion or boson star. These perturbations will excite the characteristic modes of the mixed star, so that the oscillations will be a superposition of normal modes, each one with a characteristic frequency.

By analyzing the central oscillations of the different fields, and in particular, of the central density of the star, we can study the structure of the normal modes of the fermion-boson stars. The frequencies of the normal modes are well-known for both isolated neutron and boson stars, but they have not been yet studied for mixed stars. The pulsations of compact objects are of great importance for relativistic astrophysics, because they offer the possibility of extracting information about the star (for instance the radius, mass and equation of state) from the detection of the associated gravitational waves (see [29] for a review). Although our spherical symmetry assumption only allow us to study radial modes (i.e., the fundamental mode and its overtones), it is still representative to show how these modes may change in a neutron star in the presence of a bosonic dark matter component that couples to fermions only through gravity.

We will restrict our analysis to a fermion-boson star with total mass $M_T = 1.4$, and parameterize different mixed stars by increasing the amount of bosons relative to fermions, corresponding to the fractions $N_B/N_F = \{0, 2.5, 5, 7.5, 10\}\%$. The details of the parameters of the stars are summarized in Table I. We have evolved for long times $t \approx 6000$ in order to get at least 50 oscillations of the central density, which will produce a clear spectrum with sharp peaks in the frequency domain. The Fourier

Branch	$N_B/N_F(\%)$	ϕ_c	ρ_c	ω_B	R_T	N_B	R_B	R_F
stable	0.0	0.0	1.27×10^{-3}	0.0	9.10	0.0	0.0	8.55
stable	2.5	1.33×10^{-2}	1.45×10^{-3}	0.736	8.76	0.037	6.36	8.23
stable	5.0	2.06×10^{-2}	1.67×10^{-3}	0.718	8.39	0.073	5.96	7.88
stable	7.5	2.80×10^{-2}	1.97×10^{-3}	0.694	7.99	0.107	5.52	7.50
stable	10.0	3.63×10^{-2}	2.42×10^{-3}	0.661	7.49	0.141	5.02	7.08
unstable	10.7	5.90×10^{-2}	5.05×10^{-3}	0.533	6.22	0.147	3.60	5.82

TABLE I: Properties of the fermion-boson star models used in the simulations. All the stars have a total mass $M_T = 1.4$. The columns report: the fraction of boson particles, the central value of the scalar field ϕ_c , the central density ρ_c , the internal frequency of the scalar field ω_B , the total radius of the star R_T , the number of bosonic particles N_B , and the radius of the bosonic and the fermionic components, R_B and R_F , respectively. Notice that the largest fraction of N_B/N_F for a stable configuration is reached for the maximum value of N_B and the minimum value of N_F , but the precise value of the fraction depends on the value of the total mass (in the present case we get $N_B/N_F \approx 12\%$); larger ratios N_B/N_F can be obtained for smaller values of M_T .

transform of this quantity is shown in the top panel of Fig. 9. As an additional check of our code, we can compare the known frequencies of the fundamental mode and its overtones for a (fermion-only) neutron star (as computed either by using perturbation theory or numerical evolutions, see for instance [30]) with the ones obtained from our simulation for the purely fermionic case (corresponding to the circles on the left in the bottom panel of Fig. 9). The difference is always smaller than 1%, confirming the accuracy and correctness of our results.

We now turn our attention to the boson-fermion case. The fundamental mode, which is usually a function of the mean density of the star, remains roughly constant except for the largest boson fraction, for which it shifts towards smaller frequencies. The overtones, at higher frequencies, display more interesting features with the presence of new quasi-normal modes. The original neutron star overtones, displayed with circles in Fig. 9, are the dominant ones for small number of bosons. The power of these new oscillation modes increases with the boson fraction, suggesting that their origin is the gravitational coupling with the scalar field. The frequency of the overtones has a significant drift towards higher values as the fraction of bosons increases.

The main features of this spectrum can be qualitatively explained in a very simple way. The new quasi-normal modes, which were not present for isolated fermionic stars, corresponds to the quasi-normal modes of the boson star. The oscillations in the bosonic part propagate to the fermions through gravity. As the fraction of bosons increases, so does the relative importance of the scalar field with respect to the fluid density, producing the observed growth in the amplitude of these modes. Consequently, the spectrum can be mainly understood as a superposition of the quasi-normal modes of the boson and the neutron star. The drift in the frequencies is an effect of the change in radius and mean-density of the star as the fraction of boson changes.

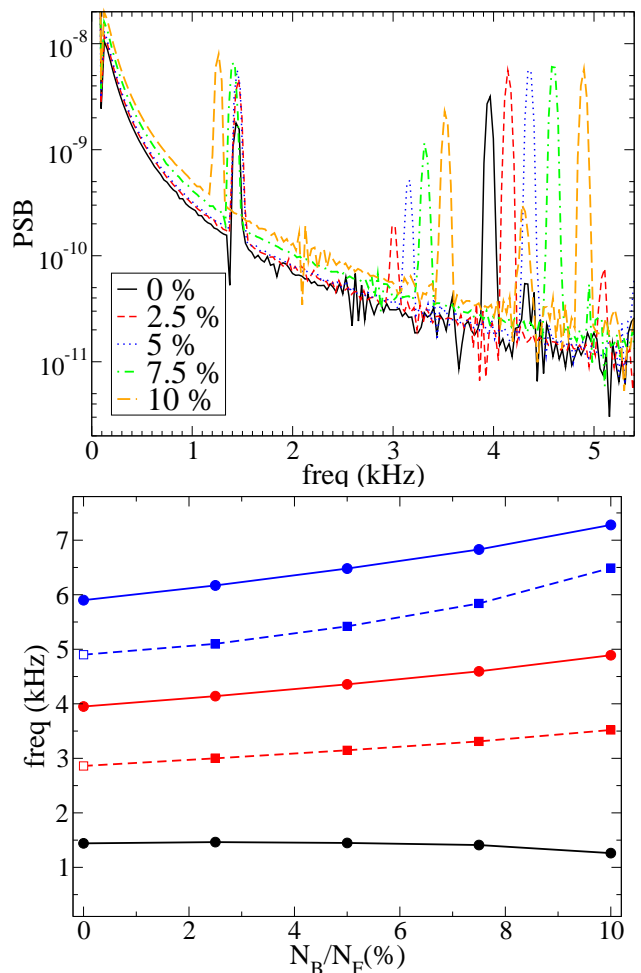


FIG. 9: Normal modes of the fermion-boson stars (Top) Fourier spectrum of the central value of the fluid density ρ_0 for several stable configuration with $N_B/N_F = \{0, 2.5, 5, 7.5, 10\}\%$ and $M_T = 1.4$. (Bottom) Frequencies corresponding to the first, second and third modes of the isolated neutron star, as a function of the boson fraction. Notice the appearance of new oscillation modes, not present for an isolated neutron star. See the text for more details.

V. CONCLUDING REMARKS

We have studied in some detail the numerical evolution of equilibrium configurations of mixed boson-fermion stars. Our results confirm the existence of stable and unstable branches of equilibrium configurations. We also defined a stability criterion based on the variation of the number of bosonic and fermionic particles, for a given fixed value of the total mass, as a function of the central values of the scalar field amplitude and the fluid density. This criterion states that the equilibrium configurations located on the left of the maximum (minimum) number of bosons (fermions) are stable, whereas the configurations located on the right are unstable. We were able to determine the curve that separates the stable branch from the unstable one, in the plane formed by the central values of the scalar field ϕ_c and fluid density ρ_c . We also verified that the correct solutions are obtained in the limiting cases of an isolated boson or fermionic star, by comparing with the results of previous studies.

In order to assess the stability criterion, we performed the numerical evolution of the fully non-linear equations of motion for two types of solutions. For the stable configuration, the central values of the scalar field and the fermionic density remain constant in time during the numerical evolution, while the unstable star migrates to a stable configuration by ejecting out some of the initial mass.

We also studied the structure of the normal modes and overtones of these mixed stars by performing long term numerical evolutions for configurations with a fixed total mass but with different boson to fermion ratios. As expected, new oscillation modes appear in the frequency spectrum of the stars, when compared to the fermion-only case; the appearance of the new overtones is justified because of the gravitational coupling of the fermionic perfect fluid with the scalar field, which has its own oscillation modes.

As we mentioned before, an accurate classification of the properties of boson-fermion stars is necessary in order to investigate the possible existence of bosons trapped inside, for instance, in neutron stars. One possible indication of such a phenomenon would be the shift in frequency and the presence of new modes in the vibration spectrum of the stars.

Another case of astrophysical interest is the possible existence of bosonic dark matter in galactic halos, an idea that has drawn some attention in the specialized

literature in recent years [23, 31–41]. This type of models refers to the other extreme case, in which the star is dominated by the bosonic component. In the context of galaxies, these mixed fermion-boson stars could model the galaxy halo with a boson star, and the gas with a fermionic component. Our present results indicate that a boson-dominated galaxy halo must keep its stability features after the inclusion of fermions; however, more work is needed to determine the properties of the equilibrium configuration that may be detected through astrophysical observations. This is work in progress that we expect to report elsewhere.

Acknowledgments

We are grateful to Juan Barranco, Cecilia Chirenti, Luis Lehner and Steve Liebling for useful comments and discussions. SV-A acknowledges support from CONACyT, México, and the kind hospitality of the Canadian Institute for Theoretical Astrophysics (CITA, Canada) for a research stay where part of this work was done. This work was partially supported by PIFI, PROMEP, DAIP-UG, CONACyT México under grant 167335, and the Instituto Avanzado de Cosmología (IAC) collaboration. DA acknowledges support from the DFG grant SFB/Transregio 7.

Appendix A: The evolution system of equations

We consider the Z3 formulation of the Einstein equations in spherical symmetry [23] as the evolution system for the space-time geometry. The system is regularized at the origin using the following transformation of the momentum constraint:

$$\tilde{Z}_r = Z_r + \frac{1}{4r} \left(1 - \frac{g_{rr}}{g_{\theta\theta}} \right),$$

which ensures the cross-cancellation of the factors $1/r$ in the fluxes, and $1/r^2$ in the sources. The sources still have terms like $1/r$ times other variables that contain radial derivatives of the metric coefficients. However, these terms do not create problems at $r \rightarrow 0$, as the radial derivatives of any differentiable function must vanish at the origin. Thus, the equations of motion read

$$\partial_t A_r = -\partial_r[\alpha \text{tr}K], \quad (\text{A1a})$$

$$\partial_t D_{rr}{}^r = -\partial_r[\alpha K_r{}^r], \quad (\text{A1b})$$

$$\partial_t D_{r\theta}{}^\theta = -\partial_r[\alpha K_\theta{}^\theta], \quad (\text{A1c})$$

$$\begin{aligned} \partial_t Z_r &= -\partial_r[2\alpha K_\theta{}^\theta] + 2\alpha \left\{ (K_r{}^r - K_\theta{}^\theta) \left(D_{r\theta}{}^\theta + \frac{1}{r} \right) - K_r{}^r \left[Z_r + \frac{1}{4r} \left(1 - \frac{g_{rr}}{g_{\theta\theta}} \right) \right] \right. \\ &\quad \left. + A_r K_\theta{}^\theta + \frac{1}{4r} \frac{g_{rr}}{g_{\theta\theta}} (K_\theta{}^\theta - K_r{}^r) - 4\pi S_r \right\}, \end{aligned} \quad (\text{A1d})$$

$$\begin{aligned} \partial_t K_r{}^r &= -\partial_r \left[\alpha g^{rr} \left(A_r + \frac{2}{3} D_{r\theta}{}^\theta - \frac{4}{3} Z_r \right) \right] + \alpha \left\{ (K_r{}^r)^2 + \frac{2}{3} K_\theta{}^\theta (K_r{}^r - K_\theta{}^\theta) \right. \\ &\quad - g^{rr} D_{rr}{}^r A_r + \frac{1}{3r} [g^{rr} (D_{rr}{}^r - A_r - 4Z_r) + g^{\theta\theta} (D_{r\theta}{}^\theta - A_r)] \\ &\quad + \frac{2}{3} g^{rr} \left[Z_r + \frac{1}{4r} \left(1 - \frac{g_{rr}}{g_{\theta\theta}} \right) \right] (2D_{rr}{}^r - 2D_{r\theta}{}^\theta - A_r) \\ &\quad \left. - \frac{2}{3} g^{rr} \left(D_{r\theta}{}^\theta + \frac{1}{r} \right) (D_{rr}{}^r - A_r) + 8\pi \left(\frac{\tau}{6} - \frac{S_r{}^r}{2} + S_\theta{}^\theta \right) \right\}, \end{aligned} \quad (\text{A1e})$$

$$\begin{aligned} \partial_t K_\theta{}^\theta &= -\partial_r \left[\alpha g^{rr} \left(-\frac{1}{3} D_{r\theta}{}^\theta + \frac{2}{3} Z_r \right) \right] + \alpha \left\{ \frac{1}{3} K_\theta{}^\theta (-K_r{}^r + 4K_\theta{}^\theta) \right. \\ &\quad + \frac{1}{6r} [g^{rr} (A_r - 2D_{rr}{}^r - 4Z_r) + g^{\theta\theta} (A_r - 2D_{r\theta}{}^\theta)] \\ &\quad - \frac{2}{3} g^{rr} \left[Z_r + \frac{1}{4r} \left(1 - \frac{g_{rr}}{g_{\theta\theta}} \right) \right] (D_{rr}{}^r - D_{r\theta}{}^\theta - 2A_r) \\ &\quad \left. + \frac{1}{3} g^{rr} \left(D_{r\theta}{}^\theta + \frac{1}{r} \right) (D_{rr}{}^r - 4A_r) + 8\pi \left(\frac{\tau}{6} - \frac{S_r{}^r}{2} + S_\theta{}^\theta \right) \right\}, \end{aligned} \quad (\text{A1f})$$

where Z_r is the vector associated with the Z3 formulation, and $\text{tr}K = K_r{}^r + 2K_\theta{}^\theta$ is the trace of the extrinsic curvature. In Sec. II we defined the matter terms of the fermionic fluid $\{D, U, \tilde{S}_r, \tilde{S}_r{}^r, \tilde{S}_\theta{}^\theta\}$, and the auxiliary variables $\{A_r, D_{rr}{}^r, D_{r\theta}{}^\theta\}$ which we introduced in order to reduce the full system in Eqs. 9, 8, and A1, to first order in space and time.

The total matter terms are given by

$$\tau = \frac{1}{2} (g^{rr} \phi_t^* \phi_t + g^{rr} \phi_r^* \phi_r + V(\phi)) + U, \quad (\text{A2a})$$

$$S_r = -\frac{1}{2} [\sqrt{g^{rr}} \phi_t^* \phi_r + \sqrt{g^{rr}} \phi_t \phi_r^*] + \tilde{S}_r, \quad (\text{A2b})$$

$$S_r{}^r = \frac{1}{2} [g^{rr} \phi_t^* \phi_t + g^{rr} \phi_r^* \phi_r - V(\phi)] + \tilde{S}_r{}^r, \quad (\text{A2c})$$

$$S_\theta{}^\theta = \frac{1}{2} [g^{rr} \phi_t^* \phi_t - g^{rr} \phi_r^* \phi_r - V(\phi)] + \tilde{S}_\theta{}^\theta. \quad (\text{A2d})$$

The total mass of the mixed stars is calculated from the ADM mass defined as

$$M_{ADM} = \frac{1}{16\pi} \lim_{r \rightarrow \infty} \int g^{pq} [\partial_q g_{pk} - \partial_k g_{pq}] N^k dS,$$

where $N^r = \sqrt{g^{rr}} \delta_r{}^r$ is the unit outward normal to the sphere. In our coordinates, it can be translated into

$$M_{ADM} = -r^2 \sqrt{g^{rr}} D g_{r\theta}{}^\theta. \quad (\text{A2})$$

For stable stars, we also use the Tolman mass defined as

$$\begin{aligned} M_T &= \int (T_0{}^0 - T_i{}^i) \sqrt{-g} dx^3, \quad (\text{A3}) \\ &= 4\pi \int r^2 \alpha \sqrt{g_{rr} g_{\theta\theta}} (\tau + S_r{}^r + 2S_\theta{}^\theta) dr. \end{aligned}$$

On the other hand, the number of fermionic particles associated to the mass of the fermionic fluid is given by

$$N_F = 4\pi \int r^2 \sqrt{g_{rr} g_{\theta\theta}} (\rho W) dr. \quad (\text{A2})$$

The number of bosonic particles can be associated to the Noether charge [1] of the scalar field, which can be computed as

$$N_B = 4\pi \int \frac{r^2}{2i\alpha} \sqrt{g_{rr} g_{\theta\theta}} (\phi^* \partial_t \phi - \phi \partial_t \phi^*) dr. \quad (\text{A2})$$

The Hamiltonian constraint takes the form

$$\begin{aligned} H &= \frac{2}{g_{rr}} \left\{ -2\partial_i D_{r\theta}{}^\theta - 3D_{r\theta}{}^\theta \left(D_{r\theta}{}^\theta + \frac{2}{r} \right) \right. \\ &\quad + g_{rr} K_\theta{}^\theta (K_\theta{}^\theta + 2K_r{}^r) - \frac{(1 - g_{rr} g^{\theta\theta})}{r^2} \\ &\quad \left. + 2D_{rr}{}^r \left(\frac{1}{r} + D_{r\theta}{}^\theta \right) - 8\pi g_{rr} \tau \right\}. \end{aligned} \quad (\text{A1})$$

Appendix B: The transformation from conserved to primitive quantities

From the definition of the conserved quantities

$$D = \rho_0 W, \quad U = hW^2 - P, \quad \tilde{S}_r = hW^2 v_r, \quad (\text{B0})$$

one obtains the primitives $\{\rho, P, v_r, \epsilon\}$ after each time integration of the equations of motion. This is not trivial, mainly because the enthalpy $h = \rho(1 + \epsilon) + P$, and the Lorentz factor $W = 1/\sqrt{1 - v^r v_r}$, are defined as functions of the primitives.

We are adopting a recovery procedure which consists in the following steps:

1. From the first thermodynamics law for adiabatic processes, it follows that

$$P = (\Gamma - 1)\rho\epsilon. \quad (\text{B0})$$

Substituting the definition of the enthalpy in the equation of state above, we write the pressure as a function of the conserved quantities and the unknown variable $x = hW^2$.

2. Using the previous step, the definition of U becomes:

$$\begin{aligned} U &= hW^2 - P \\ &= hW^2 - \frac{(\Gamma - 1)}{\Gamma}(h - \rho) \\ &= hW^2 \left(1 - \frac{\Gamma - 1}{\Gamma}\right) + \frac{\Gamma - 1}{\Gamma}\rho, \end{aligned} \quad (\text{B-1})$$

where Γ is the adiabatic index corresponding to an ideal gas.

3. Then, the function

$$f(x) = \left(1 - \frac{\Gamma - 1}{W^2 \Gamma}\right)x + \frac{D(\Gamma - 1)}{W\Gamma} - U, \quad (\text{B0})$$

must vanish for the physical solutions. The roots of the function $f(x) = 0$ can be found numerically by means of an iterative Newton-Raphson solver, so that the solution at the $n + 1$ -iteration can be computed as

$$x_{n+1} = x_n - \frac{f(x_n)}{f'(x_n)}, \quad (\text{B0})$$

where $f'(x_n)$ is the derivative of the function $f(x_n)$. The initial guess for the unknown x is given in the previous time step.

4. After each step of the Newton-Raphson solver, we update the values of the fluid primitives as

$$\rho = D/W, \quad P = x - U, \quad v_r = \tilde{S}_r/x, \quad (\text{B0})$$

where $W^2 = x^2/(x^2 - \tilde{S}_r \tilde{S}_r)$.

5. Iterate steps 3 and 4 until the difference between two successive values of x falls below a given threshold value of the order of 10^{-10} .

-
- [1] R. Ruffini and S. Bonazzola, *Phys.Rev.* **187**, 1767 (1969).
[2] Steven L. Liebling and Carlos Palenzuela, *Living Reviews in Relativity* **15** (2012), URL <http://www.livingreviews.org/lrr-2012-6>.
[3] C. Kouvaris, *Phys.Rev.* **D77**, 023006 (2008), 0708.2362.
[4] G. Bertone and M. Fairbairn, *Phys.Rev.* **D77**, 043515 (2008), 0709.1485.
[5] S. Leung, M. Chu, and L. Lin, *Phys.Rev.* **D84**, 107301 (2011), 1111.1787.
[6] A. B. Henriques, A. R. Liddle, and R. G. Moorhouse, *Phys. Lett.* **B233**, 99 (1989).
[7] L. M. Lopes and A. B. Henriques, *Phys. Lett.* **B285**, 80 (1992).
[8] A. B. Henriques and L. E. Mendes, *Astrophys. Space Sci.* **300**, 367 (2005), astro-ph/0301015.
[9] J. Breit, S. Gupta, and A. Zaks, *Phys.Lett.* **B140**, 329 (1984).
[10] A. R. Liddle, R. G. Moorhouse, and A. B. Henriques, *Classical and Quantum Gravity* **7**, 1009 (1990).
[11] T. Damour and G. Esposito-Farese, *Physical Review Letters* **70**, 2220 (1993).
[12] S. Shapiro and S. Teukolsky (1983).
[13] B. Harrison, K. Thorne, M. Wakano, and J. Wheeler, *Gravitation Theory and Gravitational Collapse* (University of Chicago Press, Chicago, 1965).
[14] N. Straumann, *General Relativity and Relativistic Astrophysics* (Springer, Berlin; New York, 1984).
[15] M. Gleiser, *Phys.Rev.* **D38**, 2376 (1988).
[16] G. B. Gelmini, M. Gleiser, and E. W. Kolb, *Phys.Rev.* **D39**, 1558 (1989).
[17] M. Gleiser and R. Watkins, *Nucl.Phys.* **B319**, 733 (1989).
[18] P. Jetzer, *Nucl.Phys.* **B316**, 411 (1989).
[19] T. Lee and Y. Pang, *Nucl.Phys.* **B315**, 477 (1989).
[20] F. V. Kusmartsev, E. W. Mielke, and F. E. Schunck, *Phys. Rev.* **D43**, 3895 (1991), 0810.0696.
[21] J. Balakrishna and F. E. Schunck (1998), gr-qc/9802054.
[22] P. Jetzer and D. Scialom (1997), gr-qc/9709056.
[23] A. Bernal, J. Barranco, D. Alic, and C. Palenzuela, *Phys. Rev.* **D81**, 044031 (2010), 0908.2435.
[24] A. B. Henriques, A. R. Liddle, and R. G. Moorhouse, *Phys. Lett.* **B251**, 511 (1990).
[25] A. B. Henriques, A. R. Liddle, and R. G. Moorhouse, *Nucl. Phys.* **B337**, 737 (1990).
[26] D. Alic, C. Bona, C. Bona-Casas, and J. Masso, *Phys. Rev.* **D76**, 104007 (2007), 0706.1189.
[27] W. H. Press, S. A. Teukolsky, W. T. Vetterling, and B. P. Flannery (1992).
[28] C.-W. Shu and S. Osher, *Journal of Computational Physics* **77**, 439 (1988).

- [29] N. Stergioulas, Living Reviews in Relativity **6** (2003), URL <http://www.livingreviews.org/lrr-2003-3>.
- [30] J. A. Font et al., Phys. Rev. **D65**, 084024 (2002), gr-qc/0110047.
- [31] L. A. Urena-Lopez, AIP Conf.Proc. **1318**, 82 (2010).
- [32] T. Matos, J. A. Vazquez, and J. Magana (2008), 0806.0683.
- [33] T. Matos and L. A. Urena-Lopez, Int.J.Mod.Phys. **D13**, 2287 (2004), astro-ph/0406194.
- [34] T. Matos and L. A. Urena-Lopez, Phys.Rev. **D63**, 063506 (2001), astro-ph/0006024.
- [35] T. Matos and L. A. Urena-Lopez, Class.Quant.Grav. **17**, L75 (2000), astro-ph/0004332.
- [36] T. Matos, F. S. Guzman, and L. A. Urena-Lopez, Class.Quant.Grav. **17**, 1707 (2000), astro-ph/9908152.
- [37] W. Hu, R. Barkana, and A. Gruzinov, Phys. Rev. Lett. **85**, 1158 (2000), URL <http://link.aps.org/doi/10.1103/PhysRevLett.85.1158>.
- [38] J.-w. Lee and I.-g. Koh, Phys. Rev. D **53**, 2236 (1996), URL <http://link.aps.org/doi/10.1103/PhysRevD.53.2236>.
- [39] S.-J. Sin, Phys. Rev. D **50**, 3650 (1994), URL <http://link.aps.org/doi/10.1103/PhysRevD.50.3650>.
- [40] V. Sahni and L. Wang, Phys. Rev. D **62**, 103517 (2000), URL <http://link.aps.org/doi/10.1103/PhysRevD.62.103517>.
- [41] A. Arbey, J. Lesgourgues, and P. Salati, Phys. Rev. D **64**, 123528 (2001), URL <http://link.aps.org/doi/10.1103/PhysRevD.64.123528>.
- [42] G. Derrick, J.Math.Phys. **5**, 1252 (1964).
- [43] G. Rosen, Journal of Mathematical Physics **7**, 2066 (1966).
- [44] Notice that, since regular and time-independent localized scalar field solutions are not stable in three spatial dimensions [42, 43], an harmonic complex scalar field is the simplest way to obtain a compact and stationary star.

